WPJET1-PR(17) 18374

W Buangam et al.

Impact of ExB flow shear stabilization on particle confinement and density peaking at JET

Preprint of Paper to be submitted for publication in
Plasma Physics and Controlled Fusion

This work has been carried out within the framework of the EUROfusion Consortium and has received funding from the Euratom research and training programme 2014-2018 under grant agreement No 633053. The views and opinions expressed herein do not necessarily reflect those of the European Commission.

Impact of ExB flow shear stabilization on particle confinement and density peaking at JET

W. Buangam[1], J. Garcia[2] and T. Onjun[3] and JET contributors*

[1]*Sirindhorn International Institute of Technology, TU, Pathumthani, Thailand*

[2]*CEA, IRFM, 13108 Saint-Paul-lez-Durance, France*

[3]*Thailand Institute of Nuclear Technology, Chatuchak, Thailand*

ABSTRACT

A deviation from the IPB98(y,2) scaling was found in dedicated power scans in the JET-ILW tokamak leading to a lower thermal energy degradation, $\tau \sim P^{-0.3}$, where τ is the energy confinement time and P is the auxiliary heating power, lower than that expected from the IPB98(y,2) scaling $\tau \sim P^{-0.69}$. In such deviations, the average density remains nearly unchanged although there is a clear density peaking increasing with auxiliary heating power. A modeling activity has been started with the CRONOS code in order to investigate the change of density peaking. By means of simulations with the quasi-linear model GLF23, a strong link between the density at the top of the pedestal and the density peaking has been found. This link can be partially explained by the well-known density peaking dependence on collisionality. However, it is found that the ExB flow shear stabilization plays an important role as it changes the particle confinement and at the same time it has a significant impact on the particle pinch direction at the vicinity of the pedestal.

Keywords: CRONOS, Bohm-GyroBohm, GLF23, positive feed-back loop, *ExB* flow shear

1. INTRODUCTION

Achieving good thermal energy confinement is a priority for the efficient production of fusion energy. However instabilities produced by microturbulence or MagnetoHydroDynamics (MHD) severely enhance perpendicular heat and particle transport leading to confinement degradation. A well-known mechanism which significantly degrades the thermal energy confinement time is the injected power, as obtained in dedicated experimental analysis, for instance the ones used for the creation of the IPB98(y,2) scaling law which leads $\tau \sim P^{-0.69}$ with P the input power. However, recent power scan experiments performed at JET-ILW [1] with neutral beam injection (NBI) power showed that the power degradation of thermal energy confinement was weaker than that expected from IPB98(y,2) scaling [2], resulting in a weak decrease of normalized thermal energy confinement at high power.

First principle modelling performed with JET C-wall discharges of core and edge regions showed several physical mechanisms that can play a role on such deviation from expected scaling laws [3]. The NBI

*See the author list of X. Litaudon et al 2017 Nucl. Fusion 57 102001

power has stabilizing effects in the core and edge regions by reducing core ion heat fluxes due to a combination of fast ions and electromagnetic effects, which reduce turbulence driven by Ion Temperature Gradient (ITG) modes, and increasing pedestal pressure due to the increased Shafranov-shift with an auxiliary heating power, which is enhanced with power due to the increase of fast ion content, which does not contribute to turbulence when the injected power is increased. In JET-ILW, the impact of electromagnetic effects and fast ions has been show to play an important role as well [4].

Whereas the reduction of heat transport by ExB flow shear in the inner part of the plasma core seems to be not dominant, the situation can be different in another plasma locations or transport channels. Gyrokinetic simulations have shown that ExB could play and important role at ρ=0.64, with ρ the normalized toroidal flux [5]. Additionally, there are indications that ExB could play a significant role on particle confinement as shown both by modeling [6] and experiments performed in DIII-D [7].

In this paper the role of ExB flow shear on particle transport and in particular on density peaking is analyzed by means of integrated modeling simulations performed with the CRONOS suite of codes [8]. For that purpose, a power scan from JET-ILW, in which there is an increase of density peaking with NBI power, is used as a way of testing the models applied and for performing dedicated ExB studies.

This work is organized as follows: brief descriptions of relevant components of the CRONOS code, together with the models applied are presented in section 2, simulation results and analyses are described in section 3; the effect of *ExB* flow shear when using GLF23 model and its impacts in density peaking are described in section 4; the effect of pedestal density when using GLF23 model and its impacts in density peaking are described in section 5; and the conclusion is given in section 6.

2. Modelling set-up

The CRONOS suite of codes is a 1D transport solver with general 2D magnetic equilibrium, for predictive simulation of a full tokamak discharge. The CRONOS code combines various modules, in which each module is responsible for computing different physical phenomena, such as transport, heating and fueling. In order to perform simulations with required physics for describing deviations from IPB98(y,2) scaling as obtained in JET-ILW power scan, models for core heat and particle transport together with pedestal top pressure must be combined. Therefore, the CRONOS suite of codes has been used for performing self-consistent simulations including core temperatures and density and edge pedestal pressure. The predictive core simulations have been carried out with two transport models, Bohm-gyroBohm [9] and GLF23 [10]. Whereas a newer version of the GLF23 model is available, called Trapped Gyro Landau Fluid (TGLF) [11], which has enhanced treatment of Trapped Electron Modes (TEM), we use here GLF23 as it has been shown that the plasmas considered in this paper are in the ITG domain [4] for which GLF23 still gives good results with JET, reproducing both temperatures an densities

with acceptable accuracy [6]. The validity of GLF23 to perform the analysis aimed in this paper will be tested by comparing the results with experimental data.

The pedestal temperature is calculated by using the so-called Cordey two-term scaling [12], which is based on an empirical scaling of pedestal stored energy. The particle transport in the pedestal region is assumed to follow ion thermal neoclassical transport and the particle sources are adjusted to match the density at the top of the pedestal for the JET-ILW discharge at 13 MW in the power scan. Once this is done, this set-up is used in all simulations in this work.

2.1 Bohm-gyroBohm core transport model

Bohm-gyroBohm is a semi-empirical anomalous transport model. It consists of a combination of Bohm and gyro-Bohm scaling. The Bohm model was first derived for electron transport [13]. Then, it was modified with a Gyro-Bohm term by adding ion transport [9]. The model can be expressed as follows

$$\chi_{e,i} = \chi_{Be,i}\langle L_{T_e}^{*}\rangle^{-1} + \chi_{gBe,i} \tag{1}$$

where $\chi_{Be,i}$ is the diffusivity of the Bohm-like model

$$\chi_{Be} = \alpha_B \frac{cT_e}{eB_t} L_{pe}^{*-1} q^2 \tag{2}$$

where $\alpha_B = 8 \times 10^{-5}$, T_e is the electron temperature, q is safety factor, e is electron charge, B_t is toroidal magnetic field, and L_{pe}^{*} is the normalized scale length of variation of electron pressure, which defined as

$$L_{pe}^{*} = \frac{p_e}{a|\nabla p_e|} \tag{3}$$

$$\chi_{Bi} = 2\chi_{Be} \tag{4}$$

while $\chi_{gBe,i}$ is a simple gyro-Bohm-like diffusivity which has the same form for electrons and ions:

$$\chi_{gB} = \alpha_{gB} \frac{cT_e}{eB_t} L_{T_e}^{*-1} \rho^{*} \tag{5}$$

$$\rho^{*} = \frac{M^{1/2} c T_e^{1/2}}{Z_i e B_t} \tag{6}$$

where $\alpha_{gB} = 3.5 \times 10^{-2}$ and L_{Te}^{*} is the normalized scale length of variation of electron temperature, which defined as

$$\langle L_{T_e}^{*}\rangle = \frac{T_e(x=0.8) - T_e(x=1)}{T_e(x=1)} \tag{7}$$

2.2 GLF23 core transport model

The GLF23 transport model is a drift-wave based model fit to linear gyrokinetic stability. It uses drift-wave linear eigenmodes to compute the quasilinear particle, thermal and toroidal and poloidal momentum transport due to ITG and TEM, although the model for TEM has been improved with TGLF, the validity of GLF23 for particle transport will be testes in this paper. It also includes the effects of ExB shear flow

reduction is also included via the reduction of the maximum growth rate with the ExB shearing as $\gamma_{net} = \gamma_{max} - \alpha_{E\times B}\gamma_{E\times B}$ where

γ_{max} is the maximum growth rate of the drift-ballooning modes in the absence of rotation shear, $\gamma_{E\times B} = (r/q)d(qV_{E\times B}/r)/dr$ is the ExB shearing rate, with a constant coefficient $\alpha_{E\times B}$ chosen through fitting to nonlinear gyrofluid simulations in the retuned version of GLF23 [10].

2.3 Pedestal Simulation

The electron density at the top of pedestal is adjusted to the experimental value. The pedestal temperature is calculated using Cordey two-term empirical based scaling [11], which can be expressed as

$$W_{ped} = 0.000643 I^{1.58} R^{1.08} P^{0.42} n^{-0.08} B^{0.06} \kappa_a^{1.81} \varepsilon^{-2.13} m^{0.2} F_q^{2.09}, \quad (8)$$

where I is the current (MA), R major radius (m), P thermal loss power (MW), n density ($10^{-19} m^{-3}$), B toroidal field (T), κ_a elongation, ε aspect ratio, m atomic mass and $F_q \left(\equiv \frac{q_{95}}{q_{cyl}} \; with \; q_{cyl} \; defined \; as \frac{5\kappa_a a^2 B}{RI} with \; a \; minor \; radius \right)$. The applicability of this scaling has been previously verified with JET and JT-60U discharges [6].

3. Power degradation simulation

In order to test whether the previous set-up modelling is adequate for analyzing JET, a validation phase has been performed. Since plasmas obtained from a power scan with a significant deviation from IPB98(y,2) scaling will be used, an immediate question is whether that deviation can be reproduced. Here the JET-ILW low triangularity scan is chosen as a test case. For these plasmas, the NBI heating deposition and fast ion pressure has been calculated with the Monte Carlo codes NEMO-SPOT [14].

Only the heat channel is simulated as the density contributes very little to the low power degradation at high power as it remains nearly unchanged with just a variation on the density peaking. Therefore, the density profile of the highest power discharge is used for the whole power scan.

The simulations are carried out using the CRONOS integrated predictive modeling code and conduct a power scan with the range used in the experiment, assuming two boundary conditions in order to evaluate the different contributions from the core or the pedestal regions to the deviation from IPB98(y,2) scaling. In one case, the temperature at the top of the pedestal is calculated using Eq. [8]; whereas for the other one, the pedestal is fixed with the value of the lower power used.

In this paper, we do not then solve momentum equation but we rather use the experimental rotation (which is measured by Charge-Exchange) and make scans on the ExB. This is done because there are strong uncertainties on the momentum diffusivity (and Prandtl number) as well as on the NBI torque (which is not measure) and it was preferred to isolate the role of ExB alone.

The main characteristics of the low triangularity JET-ILW discharge 84792 and high triangularity JET-ILW discharge 84798 are shown in Table1

Shot	Ip (MA)	Bt (T)	q_{95}	κ/δ	$\beta_N/\beta_{N,th}$	$H_{98}(y,2)$	P_{tot}(MW)
84792	1.4	1.7	4.4	1.63/0.27	2.85/2.45	1.20	13
84798	1.4	1.7	3.9	1.63/0.25	1.43/1.30	0.93	6.0

Table 1. Main characteristics of the discharges analyzed in this paper. Ip is the total current, Bt the toroidal magnetic field, κ elongation, δ triangularity, $\beta_N=\beta aB/Ip$ normalized beta (with a the plasma minor radius), $\beta_{N,th}$ normalized thermal beta, $H_{98}(y,2)$ thermal confinement factor, P_{tot} injected power.

In figure 1, the power scan performed with BGB and GLF23 (with $\alpha_{ExB} = 1.35$) models are shown. The total thermal energy is adjusted with the low $W_{th} \backsim P^{\alpha+1}$ for each case. When the pedestal follows expression 8 it is found that $\alpha = -0.40$ with BGB model whereas for GLF23 $\alpha = -0.31$. An additional scan has been performed by removing the contribution of the ExB flow shear turbulence reduction in GLF23, obtaining $\alpha = -0.48$. All these results depart from IPB98(y,2) and in the first two cases are close to the experimental result, $\alpha = -0.30$. When the contribution of the pedestal is removed, i.e. the positive feed-back loop between core and edge regions is suppressed, $\alpha = -0.51$ with BGB and $\alpha = -0.42$ and $\alpha = -0.65$ for GLF23 with and without ExB flow shear, respectively. Interestingly, with GLF23 and no ExB effects and fixed pedestal the exponent obtained is quite close to that expected from IPB98(y,2), $\alpha = -0.69$.

The results obtained are in line with first principle modelling of C-wall dsicharges [3] which showed that departure from IPB98(y,2) scaling required core turbulence stabilization and pedestal improvement both collinear with power.

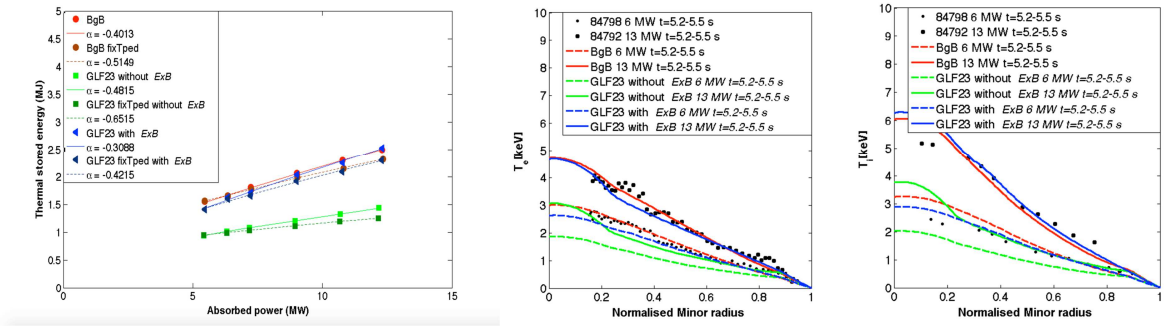

Figure1. Plasma thermal stored energy as a function of absorbed heating power with difference core and edge transport model setting. The solid and dash line are fits to the data assuming a scaling of the form $W_{th} \backsim P^{\alpha+1}$ for fixed and evolving pedestal temperature where α is the exponent for the scaling for energy confinement time with power (left). Electron (center) and ion (right) temperature profiles averaged

for 5.2-5.5s at two power levels for each of the six power scans by using Bohm-GyroBohm (red) and GLF23 without ExB (green) and GLF23 with ExB (blue) core transport model. The average experimental values for 5.2-5.5s obtained from High Resolution Thomson Scattering (HRTS) and Charge Exchange (CX) are plotted with dots.

4. THE EFFECT OF $\boldsymbol{E \times B}$ FLOW SHEAR AND ITS IMPACT ON DENSITY PEAKING

An important point obtained in the experimental power scan is that the line average density did not change but the density peaking changed with power. This can be shown by comparing the values of the normalized electron density gradient, $L_n = -R\nabla n_e/n_e$, being R the major radius, for the high power case (#84792) with P=13.0 MW and low power case (#84798) with P=6.0 MW. For the discharge 84792, $L_n(\rho = 0.33) = 1.22$ and $L_n(\rho = 0.85) = 7.53$ whereas for the discharge 84798, $L_n(\rho = 0.33) = 0.89$ and $L_n(\rho = 0.85) = 4.12$.

Several physical mechanisms can have an impact on such peaking, as the different collisonallity, which is known to have an impact on density peaking [15] due to the change in turbulent mode structure, or ELM frequency which can change the particle sink or the NBI fueling. In this paper, however, a systematic analysis of the impact of the ExB flow shear stabilization on particle confinement is going to be performed.

For that purpose, several scans will be performed in self-consistent simulations including heat and particle transport and the resulting density peaking will be analyzed and compared to that expected from the scaling proposed in Ref. [15], which is regularly used to perform predictions of density peaking.

As a first step, a simulation (with GLF23) including T_e, T_i and n_e (with fitted experimental rotation profiles shown in figure 2) at injected powers P=13MW and P=5MW is performed and the density profiles obtained are compared to experimental data obtained from HRTS. The electron density at the top of the pedestal has been matched by assuming that the particle transport is reduced to ion neoclassical thermal transport in the pedestal region and by varying the amount of cold neutrals (which follow a Gaussian profile). Regarding the impact of ExB flow shear stabilization, the value $\alpha_{ExB} = 1.35$ has been chosen in this initial simulation. In figure 2, the electron density obtained is compared to experimental data. The increasing in density peaking with power is well reproduced by the modelling whereas the absolute density peaking of the high power discharge is slightly overestimated as it was found as well for hybrid discharges, which showed an overestimation of the thermal confinement mainly when ExB flow shear was included [16].

An important difference from both discharges is that the difference in density peaking already starts next to the pedestal region precisely where significant differences have been found in the particle pinch, as shown as well in figure 2. Whereas in both simulations the pinch is positive (i.e. inward), it is ten times

higher for the high power case at $\rho = 0.8$ that for the low power one. Another important feature is that the pinch is much higher next to the pedestal region than in the inner core, where it is almost negligible.

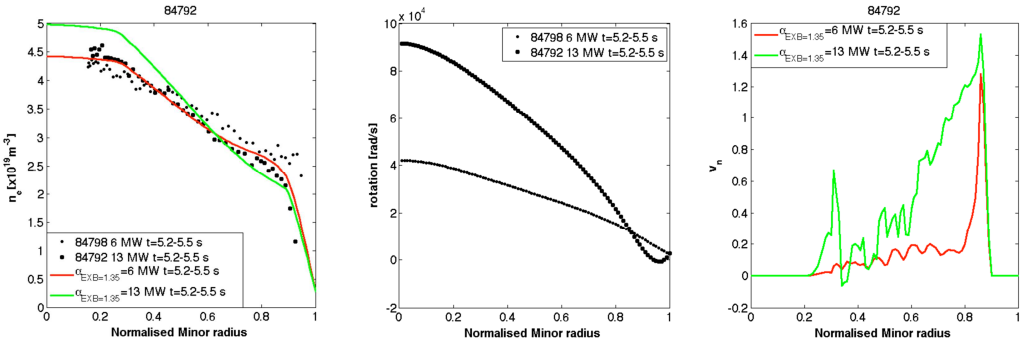

Figure2. The average electron density profiles (left) , average experimental rotation profile (center) and average pinch velocity profile (right) from 5.2-5.5 s obtained in the full self-consistent simulation.

In order to have a deeper insight on the role of ExB on particle confinement and density peaking, a scan on ExB flow shear has been performed by changing the value of α_{ExB}. In figure 3, the ion and electron temperatures profiles obtained are shown whereas in figure 4 the electron density profiles also shown for each value of α_{ExB}. There is a clear degradation of confinement when decreasing ExB flow shear accompanied as well with a decreasing of the density peaking. Actually, the impact of ExB is stronger in the particle channel than in the heat channel. The change in the density peaking starts next to the pedestal, where a local change of peaking is very evident, although the absolute value of the density does not significantly change. In order to analyze this aspect, in figure 4 the particle pinch is plotted for all the cases considered. Surprisingly, there is a reversal of the particle pinch in the edge region from inward for $\alpha_{ExB} = 1.35$ to outward for $\alpha_{ExB} = 0.2$. Whereas there is still a density peaking at mid radius for all the cases considered, the impact of the local change of density peaking in the pedestal region propagates to the core reducing the global peaking.

In order to analyse these results, they are compared to well-known scaling laws for the density peaking from [14].

The scaling used in this paper for comparison is:

$$n_{e,peaking} = \frac{n_{e(\rho=0.2)}}{\langle n_e \rangle} = 1.345 \pm 0.014 - (0.115 \pm 0.005) log\left(\nu_{eff}\right) + (1.168 \pm 0.010)\Gamma^*_{NBI} - (4.262 \pm 0.810)\beta \quad (9)$$

where $\langle n_{e,vol} \rangle = \frac{\int_0^1 n_e dV}{\int_0^1 dV}$, $\nu_{eff} = \frac{0.2\langle n_e \rangle R_{geo}}{\langle T_e \rangle^2}$, $\beta = 4.02x10^{-3}\langle p \rangle / B_T^2$.

In these formulae, densities are in 10^{19}m^{-3}, temperatures are in keV, magnetic fields are in Tesla, the total plasma pressure p is in keVx10^{19}m^{-3}, the symbol $\langle \quad \rangle$ denotes as a volume average, and Γ^*_{NBI} is the source contribution due to the beams.

In table 2, the values of the density peaking obtained in the simulations are compared to the results from

Eq. [9]. Additionally, the values of $\nu_{eff}, \beta \; and \; \Gamma^{*}_{NBI}$ are also shown. Whereas the density peaking from the simulations increases from 1.42 for $\alpha_{ExB} = 0$ up to 1.65 for $\alpha_{ExB} = 1.35$ the results from the scaling remain unchanged, with a value of $n_{e,peak} \approx 1.50$, for any ExB indicating that no variation of density peaking would be expected. In this case, the ExB provides an additional physical mechanism to the density peaking which is not covered by the scaling. This also means that there is a general coupling for the core and edge plasma regions regarding particle transport as core density is partially determined by edge ExB characteristics.

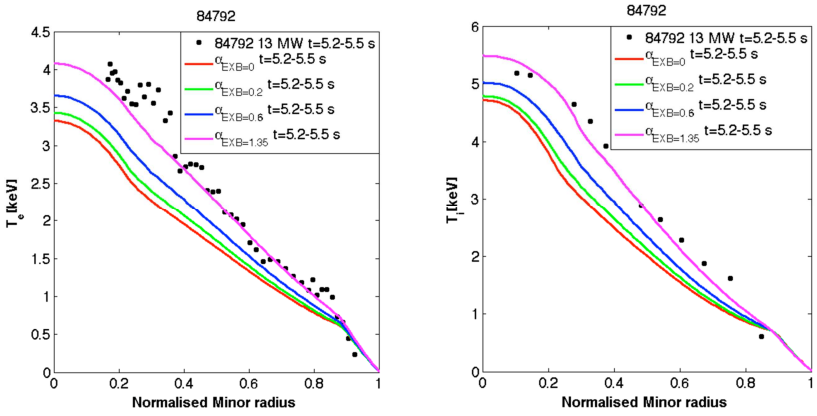

Figure3. The average electron (left) and average ion (right) temperature profiles from 5.2-5.5 s obtained in the full self-consistent simulation for different α_{ExB} values

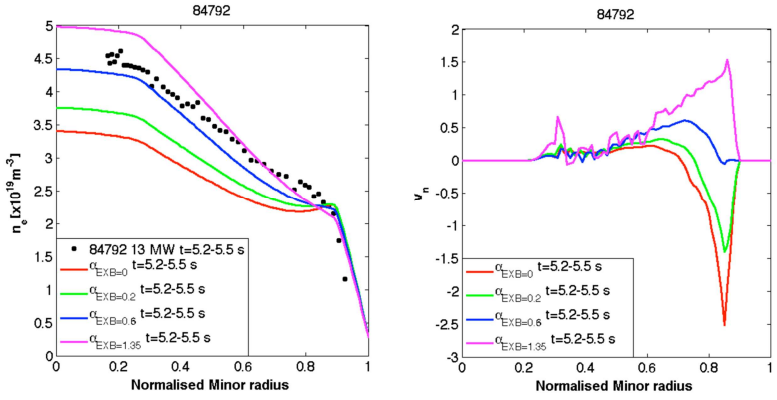

Figure4. The average electron density profiles (left) and average pinch velocity (right) from 5.2-5.5 s for different α_{ExB} values

ExB flow shear	$\alpha_{E\times B} = 0$	$\alpha_{E\times B} = 0.2$	$\alpha_{E\times B} = 0.6$	$\alpha_{E\times B} = 1.35$
Density peaking	1.42	1.47	1.57	1.65
Peaking from scaling	1.50	1.49	1.49	1.48
v_{eff}	0.72	0.87	0.79	0.64
$\beta[\%]$	0.79	0.91	1.1	1.5
Γ^*_{NBI}	0.151	0.151	0.151	0.151

Table2. Electron density peaking defined as $\frac{n_{e(\rho=0.2)}}{\langle n_e \rangle}$, where $\langle n_{e,vol} \rangle = \frac{\int_0^1 n_e dV}{\int_0^1 dV}$, obtained for the different ExB flow shear used.

The effect of NBI fueling, which is known to play a role as well on the density peaking [6,17,18], has been analyzed too by artificially rescaling the NBI fueling obtained in the integrated modelling simulation and assuming experimental toroidal rotation and $\alpha_{E\times B} = 1.35$. In figure 5, the density profiles and the pinch obtained are shown for three cases with different rescaling factor. The resulting density peaking is shown in table 3. In this case, whereas there is a significant decreasing in the total density, the impact on peaking is weak and there is no impact at all on the particle pinch. Unlike previous scans on ExB, the scaling follows the same trend with a weak decreasing density peaking.

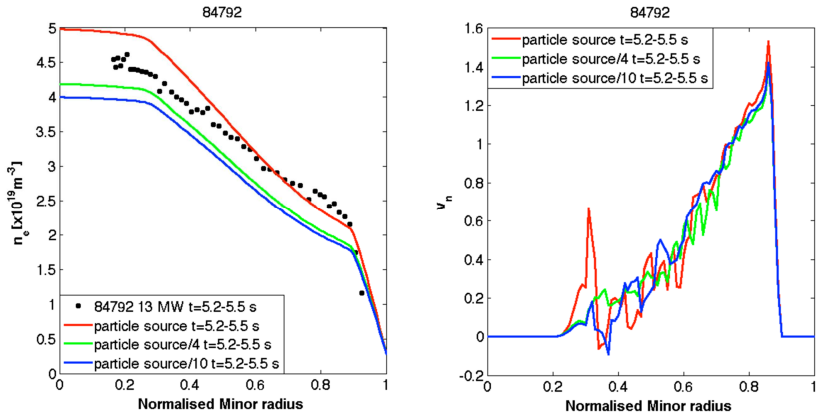

Figure5. The average electron density profiles and average pinch velocity profile from 5.2-5.5 s at different NBI fueling for $\alpha_{E\times B} = 1.35$

NBI fueling	particle source	particle source/4	particle source/10
Density peaking	1.65	1.62	1.61
Peaking from scaling	1.42	1.31	1.28
v_{eff}	0.64	0.44	0.40
$\beta[\%]$	2.95	2.91	2.90
Γ^*_{NBI}	0.151	0.03775	0.0151

Table3. Electron density peaking obtained for the different NBI fueling used.

5. THE EFFECT OF PEDESTAL DENSITY AND ITS IMPACT ON DENSITY PEAKING

Two main different mechanisms have identified here playing a role on particle confinement and density peaking, i.e. collisisonality and edge ExB flow shear stabilization. In particular, edge conditions play a significant role. Therefore, a strong link between core density and pedestal density could be expected as pedestal density highly determines global collisionality and at least at JET, the pedestal density also highly impacts on the Neutral Beam Injection ionization and therefore torque (which is one of the main sources of ExB flow shear).

In order to explore the link between pedestal density and density peaking a scan on the pedestal top density has been performed by artificially changing the pedestal particle transport. This scan is done for different values of $\alpha_{E\times B}$ in order to get a trend between the interplay between collisionality and ExB.
In figures 6, 7 and 8, the scans are shown for $\alpha_{E\times B} = 0.2$, $\alpha_{E\times B} = 0.6$ and $\alpha_{E\times B} = 1.35$, respectively; whereas the results are detailed shown in table 4. There is a clear trend on decreasing the density peaking with increasing pedestal top density. This trend is associated with a significant change on the particle pinch from positive to negative which is associated to a change on collisionality as shown in table 4. This general trend is well recovered using the scaling from equation 9.
However, the general trend is modified by each value of $\alpha_{E\times B}$, as it changes the pinch from mostly positive values regardless the pedestal density for $\alpha_{E\times B} = 1.35$ to significant negative ones for $\alpha_{E\times B} = 0.2$. The different trend for different $\alpha_{E\times B}$ is summarized in figure 9 where the dependence of the density peaking, $n_{e,peaking}$, and line average density, $n_{e,l}$ on the pedestal density is adjusted to a power law of the type $n_{e,ped}^{\gamma}$. For $n_{e,peaking}$, $-0.226 < \gamma < -0.158$ is obtained when $\alpha_{E\times B}$ is changed from $\alpha_{E\times B} = 0.2$ up to $\alpha_{E\times B} = 1.35$ whereas for $n_{e,l}$, $0.526 < \gamma < 0.654$ for the same range of $\alpha_{E\times B}$. This shows that significant deviations from a general trend on collisionality are expected depending the ExB flow shear levels at the edge region. This is particularly important for ITER extrapolations, as from a pure collisionality dependence, the density peaking expected should be very high, however, due to the modest ExB flow shear level expected as well the density peaking might lower than general expectations. This possibility will be analyzed in the future.

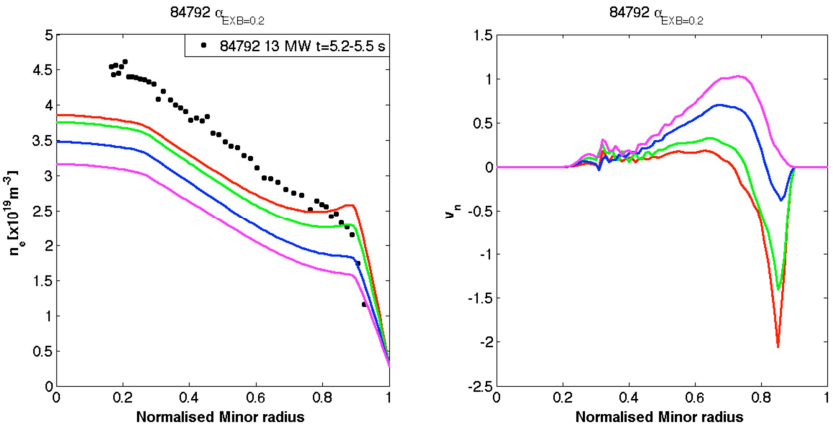

Figure6. Pedestal density scan for 13 MW averaged in 5.2-5.5 s for $\alpha_{E\times B} = 0.2$ (left) and the corresponding (with the same color as for the density) averaged pinch velocity (right).

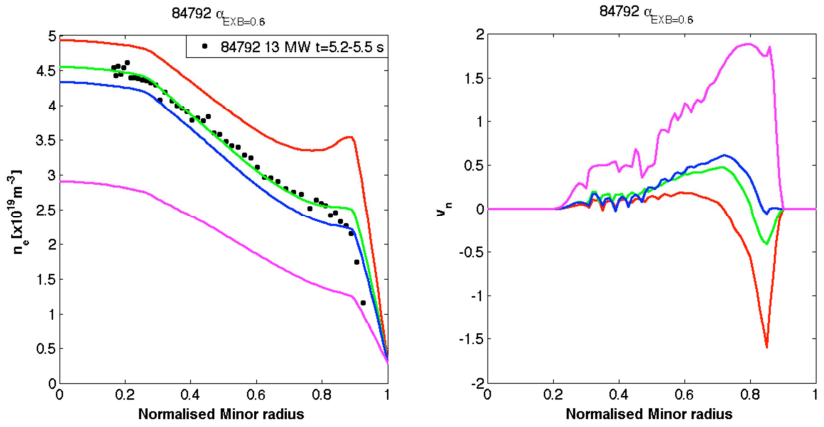

Figure7. Pedestal density scan for 13 MW averaged in 5.2-5.5 s for 13 MW with $\alpha_{E\times B} = 0.6$ (left) and the corresponding (with the same color as for the density) averaged pinch velocity (right)

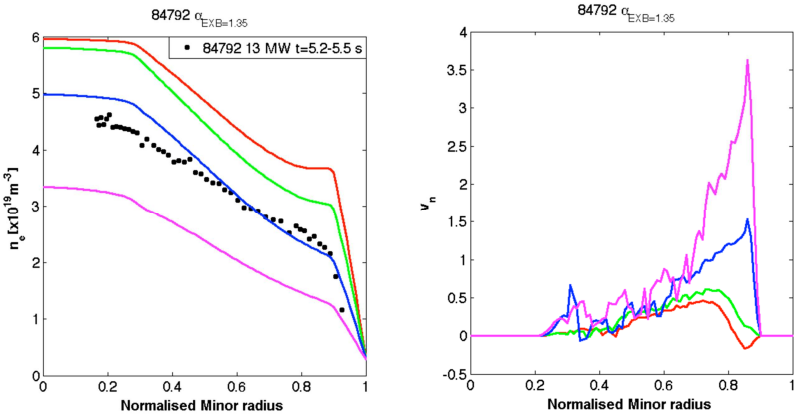

Figure8. Pedestal density scan for 13 MW averaged in 5.2-5.5 s for 13 MW for $\alpha_{E\times B} = 1.35$ (left) and the corresponding (with the same color as for the density) averaged pinch velocity (right)

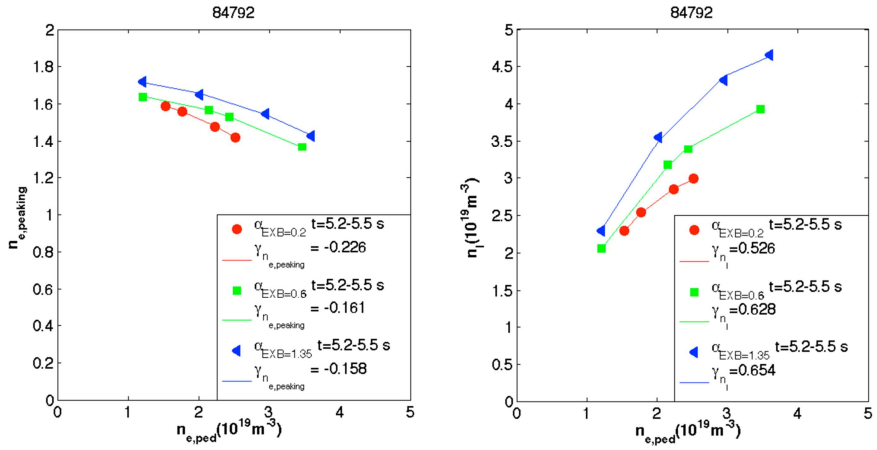

Figure9. Density peaking (left) and line average (right) electron density dependence on the pedestal density for $\alpha_{E\times B} = 0.2, 0.6\ and\ 1.35$

$\alpha_{E\times B} = 0.2$	Density peaking	Peaking from scaling	v_{eff}	β[%]	Γ^*_{NBI}
	1.42	1.48	1.03	0.90	0.151
	1.48	1.49	0.87	0.91	0.151
	1.56	1.51	0.62	0.91	0.151
	1.59	1.52	0.48	0.89	0.151
$\alpha_{E\times B} = 0.6$	Density peaking	Peaking from scaling	v_{eff}	β[%]	Γ^*_{NBI}
	1.37	1.46	1.37	1.19	0.151
	1.53	1.48	0.93	1.14	0.151
	1.57	1.49	0.79	1.12	0.151
	1.64	1.54	0.28	1.03	0.151
$\alpha_{E\times B} = 1.35$	Density peaking	Peaking from scaling	v_{eff}	β[%]	Γ^*_{NBI}
	1.43	1.44	1.10	1.76	0.151
	1.55	1.45	0.94	1.66	0.151
	1.65	1.49	0.64	1.31	0.151
	1.72	1.54	0.25	1.26	0.151

Table4. Electron density peaking for different values of $E \times B$ flow shear and pedestal density.

6. SUMMARY AND CONCLUSIONS

A modelling activity has been carried out in order to investigate the different mechanisms by which the density is peaked in JET-ILW experiments. For that purpose, integrated modelling has been used for performing predictive heat and particle predictions which have been compared with profiles obtained from JET power scans showing a significant deviation from IPB98(y,2) scaling.

In general, the models considered in this paper are able to reproduce deviations from IPB98(y,2) showing that improved core confinement (collinear with the input power) and pedestal increasing with power are necessary ingredients for this deviation. The increased density peaking obtained with power is also recovered.

It has been shown that a significant contribution for such density peaking comes from the dependence of particle transport on the ExB flow shear stabilization. By mean of ExB flow shear scan, it has been shown that there is a direct correlation between the particle pinch within the pedestal region and the global particle confinement and the density peaking. This trend cannot be recovered by using the typical scaling on colisionality as there is no dependence on ExB. Such mechanism is primarily an edge effect that propagates to the core. On the other hand, the impact of ExB on particle transport in the inner part of the core is less important.

In general, density peaking increasing with lower collisionality has been recovered by performing pedestal density scan, however, the ExB flow shear stabilization introduces deviations from the scaling. This is particular important for ITER extrapolations. A high density peaking would be expected from its low collisionality. However, the low torque (and likely ExB) and the low NBI fueling can lead to some significant deviation, decreasing the expected peaking.

Finally, the modelling shown in this paper does not give the physical mechanisms by which the pinch significantly changes its sign with ExB. Whereas some indications of pinch reversal have been obtained in gyrokinetic simulations, the impact of ExB has not been analyzed [19]. This will be done in the future by extending the present analysis to non-linear gyrokinetic simulations.

ACKNOWLEDGEMENT

This project is supported by The Franco-Thai scholarship program and Development and Promotion of Science and Technology Talents Project.

“This work has been carried out within the framework of the EUROfusion Consortium and has received funding from the Euratom research and training programme 2014-2018 under grant agreement No 633053. The views and opinions expressed herein do not necessarily reflect those of the European Commission.”

REFERENCES

[1] C. Challis et al., Nucl. Fusion 55 (2015) 053031

[2] D C McDonald et al., Plasma Phys Control Fusion 46 (2004) A215

[3] J. Garcia et al., Nucl. Fusion 55 (2015) 053007

[4] H. Doerk et al., Plasma Phys Control Fusion 58 (2016) 115005

[5] J. Citrin et al., Plasma Phys Control Fusion 57 (2015) 014032

[6] J. Garcia et al., Nucl. Fusion 54 (2014) 093010

[7] X. Wang et al., Plasma Phys Control Fusion 58 (2016) 045026

[8] J. F. Artaud et al., Nucl. Fusion 50 (2010) 043001

[9] M. Erba et al., Plasma Phys Control Fusion 39 (1997) 261-276

[10] J.E. Kinsey et al., Phys Plasmas 12 (2005) 052503

[11] G.M. Staebler et al., Phys. Plasmas 12 (2005) 102508

[12] J.G. Cordey et al., Nucl. Fusion 43 (2003) 670-4

[13] A. Taroni et al., Plasma Phys Control Fusion 36 (1994) 1629

[14] M. Schneider et al., Nucl. Fusion 51 (2011) 063019

[15] C. Angioni et al., Nucl. Fusion 47 (2007) 1326-1335

[16] I. Voitsekhovitch Nucl. Fusion 54 (2014) 093006

[17] L. Garzotti et al., Nucl. Fusion 46 (2006) 994-1000

[18] T. Tala et al., "Density peaking in JET-Driven by Fueling or Transport?" 26th IAEA Fusion Energy Conference Kyoto, Japan 17-22 October 2016 https://nucleus.iaea.org/sites/fusionportal/Shared%20Documents/FEC%202016/fec2016-preprints/preprint0403.pdf

[19] D.R. Mikkelsen et al Physics of Plasmas 22, 062301 (2015)